ADVANCED OPTICAL MATERIALS
www.advopticalmat.de

Comparison of Harmonic Generation from Crystalline and Amorphous Gallium Phosphide Nanofilms

Benjamin Tilmann, Tahiyat Huq, Thomas Possmayer, Jakub Dranczewski, Bert Nickel, Haizhong Zhang, Leonid Krivitsky, Arseniy I. Kuznetsov, Leonardo de S. Menezes, Stefano Vezzoli, Riccardo Sapienza,* and Stefan A. Maier**

Gallium phosphide (GaP) is a promising material for nanophotonics, given its large refractive index and a transparency over most of the visible spectrum. However, since easy phase-matching is not possible with bulk GaP, a comprehensive study of its nonlinear optical properties for harmonic generation, especially when grown as thin films, is still missing. Here, second harmonic generation is studied from epitaxially grown GaP thin films, demonstrating that the absolute conversion efficiencies are comparable to a bulk wafer over the pump wavelength range from 1060 to 1370 nm. Furthermore, the results are compared to nonlinear simulations, and the second order nonlinear susceptibility is extracted, showing a similar dispersion and magnitude to that of the bulk material. Furthermore, the third order nonlinear susceptibility of amorphous GaP thin films is extracted from third harmonic generation to be more than one order of magnitude larger than that of the crystalline material, and generation of up to the fifth harmonic is reported. The results show the potential of crystalline and amorphous thin films for nonlinear optics with nanoantennas and metasurfaces, particularly in the visible to near infrared part of the spectrum.

1. Introduction

On the macroscopic scale, efficient nonlinear frequency generation is mainly determined by low intrinsic optical losses, a small phase-mismatch between interacting waves, together with a high intrinsic nonlinear coefficient.[1] Therefore, common nonlinear crystals are transparent and optically birefrigent, with popular examples being barium borate (BBO), lithium niobate ($LiNbO_3$) or potassium titanyl phosphate (KTP). For nanophotonic applications, where the interaction volumes are comparable to the scale of the operating wavelengths, the material requirements shift due to the relaxation of phase matching conditions found in bulk nonlinear optics.[2,3] Here, a large linear refractive index is highly beneficial to enable photonic engineering, while large nonlinear susceptibilities are needed to compensate for the small interaction volumes. Finally, experimental realization and technical applications need ease-of-integration with common nanofabrication and ideally silicon photonic techniques. Noble metals are one focus of interest due to their plasmonic resonances and high nonlinear coefficients.[4–6] However, the high ohmic losses and low damage threshold of metallic particles limit their applications particularly for nonlinear optics.[7] On the other hand, dielectric materials can serve as an alternative

B. Tilmann, T. Possmayer, L. de S. Menezes, S. A. Maier
Chair in Hybrid Nanosystems, Nanoinstitut München, Fakultät für Physik
Ludwig-Maximilians-Universität München
80539 München, Germany
E-mail: b.tilmann@physik.uni-muenchen.de; stefan.maier@monash.edu

T. Huq, J. Dranczewski, S. Vezzoli, R. Sapienza, S. A. Maier
The Blackett Laboratory, Department of Physics
Imperial College London
London SW7 2AZ, UK
E-mail: r.sapienza@imperial.ac.uk

B. Nickel, L. de S. Menezes
Departamento de Física
Universidade Federal de Pernambuco
Recife-PE 50670-901, Brazil

H. Zhang, L. Krivitsky, A. I. Kuznetsov
Insitute of Materials Research and Engineering, A*STAR (Agency for Science, Technology and Research)
Singapore 138634, Singapore

B. Nickel
Fakultät für Physik and Center for NanoScience (CeNS)
Ludwig-Maximilians-Universität
80539 München, Germany

S. A. Maier
School of Physics and Astronomy
Monash University
Clayton VIC 3800, Australia

The ORCID identification number(s) for the author(s) of this article can be found under https://doi.org/10.1002/adom.202300269

DOI: 10.1002/adom.202300269

and versatile platform with ultralow losses, widely tunable Mie resonances and a good compatibility with silicon fabrication techniques.[7,8] Among this material family, gallium phosphide (GaP) is a prominent example, well-known in the light-emitting diode industry.[9] Its large bandgap of 2.25 eV[10] grants a virtually lossless transparency window for wavelengths longer than ≈550 nm while its refractive index larger than 3.2–3.5 is one of the largest among dielectric materials. First promising results were reported by nanostructuring bulk GaP crystals for efficient second-harmonic generation (SHG),[11–14] the coupling to 2D materials,[15,16] surface-enhanced fluorescence[11] or photonic crystals.[17] However, fabrication from the bulk crystal naturally limits the refractive index contrast in the substrate direction and additionally prevents direct on-chip fabrication. Nevertheless, recent studies were focused on GaP thin films with amorphous or crystalline structure, depending on the deposition method. Single GaP nanostructures on transparent substrates were shown to generate record-value performances for all-optical switching,[18,19] nonlinear integrated photonics[20] and nanophotonic engineering with dielectric metasurfaces.[21–23] However, so far an in-depth characterization of the nonlinear optical properties of GaP thin films is missing, in particular regarding the spectral shape and polarization dependence of the fundamental beam.

In this work, we present a thorough analysis of the linear and nonlinear optical properties of crystalline GaP (c-GaP) thin films. We show that the high quality of a 410 nm thin film allows strong SHG over a broad wavelength range spanning from 1.06 to1.37 µm, reaching absolute frequency conversion efficiencies comparable to that of a bulk GaP crystal. Using nonlinear scattering theory coupled with transfer-matrix method (TMM) simulations, we determine the value of the second-order nonlinear susceptibility to be $\chi_{eff}^{(2)} \simeq 60$ pm V^{-1} with a weak spectral dependence, agreeing well with literature values.[24] We furthermore show that the amorphous structure of sputtered GaP films (a-GaP) prevents significant SHG, while third-harmonic generation (THG) is possible with high efficiency. Under excitation with 1.65 µ m wavelength light, we extract a high third-order nonlinear susceptibility of $\chi_{eff}^{(3)} \simeq 3 \cdot 10^{-19}$ m^{2}V^{-2}, one order of magnitude larger than for the crystalline samples, which we believe is mainly due to a higher linear refractive index. Besides this, up to fifth harmonic generation has been observed for all GaP samples, while for the centrosymmetric a-GaP film no even order-harmonic signal could be detected.

These results strengthen the promise of GaP as a viable candidate for nanophotonics. The fact that c-GaP thin films perform comparable to the bulk crystal makes them well-suited for second-order nonlinear applications, particularly in the visible part of the spectrum. On the other hand, a-GaP films promise to perform even better than the crystalline counterparts and outperform many common nonlinear materials when looking at third-order nonlinear processes. Altogether, optical devices based on GaP thin films can cover a broad range of excitation wavelengths, including most of the visible spectrum, and therefore present a versatile platform for nonlinear on-chip applications.

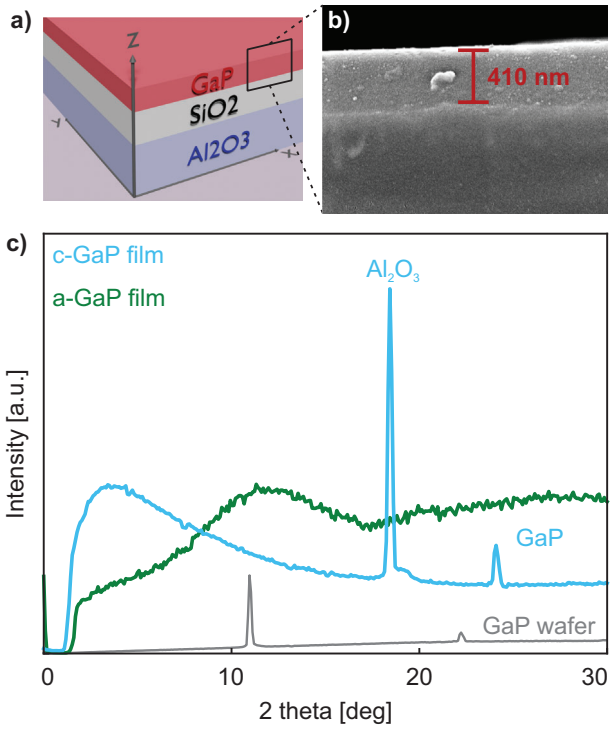

Figure 1. a) Scheme of the investigated sample, consisting of an Al_2O_3 substrate, a layer of SiO_2 and the c-GaP film. The *x* and *y* axes correspond to the [100] and [010] crystal axes, respectively, while the [100] axis is tilted with respect to the *z*-axis. b) SEM image of the sample edge, clearly showing the GaP layer on top of the SiO_2. c) XRD measurements of crystalline GaP film (blue) and an amorphous GaP film (green). In grey, a reference measurement of a bulk [111] oriented GaP wafer is shown.

2. Results and Discussion

Optical SHG is the most prominent example of second-order nonlinear phenomena, where two incident photons of frequency f_0 get converted to a new photon with exactly double the frequency $2 \times f_0$. This process is only allowed if light travels through a nonlinear medium with non-vanishing second-order susceptibility $\chi^{(2)}$. The second-order nonlinear polarization is described by[1]

$$P_i^{(2)} = \chi_{ijk}^{(2)} E_j E_k \tag{1}$$

with *i*, *j*, *k* running over the spatial coordinates *x*, *y*, *z*. Generally, $\chi_{ijk}^{(2)}$ is a rank-3 tensor that is highly sensitive to the symmetries present in the material, for example, it completely vanishes in all centro-symmetric materials.[25] GaP can be deposited with different techniques, resulting in either in a centrosymmetric amorphous phase (a-GaP) with vanishing $\chi^{(2)}$ or in a crystalline zincblende structure (c-GaP), where second-order nonlinear effects are possible. To obtain high-quality c-GaP films, our samples are fabricated via metal-organic vapor-phase epitaxy growth on top of a gallium arsenide (GaAs) carrier wafer.[26] Subsequently, a transfer direct bonding to a sapphire (Al_2O_3) substrate using 2 µm layer of SiO_2 as buffer layer and the removal of the carrier wafer results in the material stack sketched in **Figure 1**a.

A high homogeneity of the layers and the clear distinction of c-GaP to the SiO_2 layer below is confirmed by a scanning electron microscopy (SEM) cross section, shown in Figure 1b. Moreover, the X-ray diffraction (XRD) measurements that are shown by the green curve in Figure 1c proof the crystalline order of the film. Although there is an amorphous background generated by the underlying SiO_2 layer and a strong XRD peak from the sapphire substrate, the peak at $2\theta \simeq 24°$ can be attributed to the c-GaP thin film. This differs markly to the clear amorphous XRD signal of an a-GaP film, shown by the blue line in Figure 1. It should be noted that in order to minimize the lattice mismatch, the c-GaP layer is grown with the [001] crystal plane tilted with respect to the surface normal. Therefore, the peak appears shifted compared to a reference GaP wafer, cut along the [111] crystal direction and shown in grey in Figure 1c. Here, the peak positions are in excellent agreement with literature values.[27].

The zincblende structure of the GaP crystal corresponds to the $\bar{4}3m$ symmetry class. This allows to reduce the elements of the $\chi^{(2)}$ tensor from Equation 1, where most elements vanish and only the off-diagonal elements remain and are all identical.[25]

$$\chi^{(2)}_{eff} = \chi^{(2)}_{xyz} = \chi^{(2)}_{xzy} = \chi^{(2)}_{yxz} = \chi^{(2)}_{yzx} = \chi^{(2)}_{zxy} = \chi^{(2)}_{zyx} \tag{2}$$

From this follows that a GaP crystal illuminated normal to the [001] crystal surface, does not generate SHG light and the material behaves as quasi centro-symmetric.[28] This however changes when the illumination is no longer perpendicular to the crystal axes and a rotation matrix has to be applied to the tensor in order to describe the system (refer to Supporting Information for more details). Since this is the case for the c-GaP film and the [111] oriented GaP wafer, SHG signal can be detected under normal incidence. **Figure 2**a,b, respectively, show the measured SHG efficiency $\eta \propto \frac{I_{SHG}}{I^2_{pump}}$ for both materials at fundamental wavelengths ranging from 1.06 to1.37 µm. It should be noted that we are here using the so-called power normalized efficiency instead of the absolute conversion efficiency $\eta \propto I_{SHG}/I_{pump}$, which scales linearly with the pump intensity. I_{SHG} and I_{pump} refer to the measured peak intensities of SHG and pump light, respectively. The collection of the generated light is performed in transmission geometry while I_{SHG} and I_{pump} are determined from the measured average powers, the laser repetition rate and temporal pulse width, normalized by the beam size as measured with a knife-edge technique. A power dependence measurement that can be found in Supporting Information shows the expected quadratic behavior and therefore confirms the second-order nonlinear nature of the measured signal. The SHG efficiency of the c-GaP film (Figure 2b) shows an oscillatory behavior that peaks around 1.25 µm where it compares well to the values measured for the GaP wafer (Figure 2a). For longer wavelengths, however, the bulk efficiency can almost double while the thin film reduces to only 10% of that value. This is consequence of the fact that GaP is completely transparent over the relevant spectral range and both samples are fully penetrated by the pump light. Therefore, one important property to determine the SHG efficiency is the linear transmission of the samples, shown in Figure 2c,d. The optically thick GaP wafer (Figure 2c), does not show significant spectral features, particularly not in the regime of the pump wavelength (top panel). Only in the SHG regime (bottom panel), the position of the indirect bandgap at 550 nm (lower panel), leads to a fast drop in the transmission, which however, does not have visible impact on the observed SHG efficiency. Therefore, the continuous growth that is measured for η_{SHG} cannot be attributed to the transmission itself, but can be explained by the coherence length of the SHG light that scales with the wavelength of the appearing light.[29] For the thin film on the other hand, coherence length and phase-matching in general are subordinate, and the linear transmission is dominant (Figure 2d). Here, the small thickness leads to strong thin film Fabry–Perot oscillations, with two observable oscillation periods. A shorter one is induced by the thick SiO_2 spacer while the 410 nm GaP layer is responsible for the long-period oscillation. Consequently, the recorded SHG efficiency embodies a product of the transmittance at fundamental and SHG wavelengths leading to the observed oscillatory course.

The dashed black lines in Figure 2c,d represents numerical simulations of the transmission based on the transfer matrix method[30] with the complex linear refractive index of GaP as input parameter. These values are extracted from spectral ellipsometry measurements of the GaP wafer (see Supporting Information). It should be noted that the birefrigence of the sapphire substrate prevents a direct measurement of the optical constants for the c-GaP film with this method. The nevertheless excellent agreement between measurement and numerical model underlines the high quality and optical similarity of the grown thin film to bulk GaP.

Based on two linear simulations, a nonlinear model of the SHG process can now be built in order to extract the second-order nonlinear susceptibility. In accordance with nonlinear scattering theory,[30] the simulated SHG electric field $E_{SHG,\,model}$ collected at the detector position can be calculated as:

$$E_{SHG,model}(\omega) \propto \int_{V_{film}} \chi^{(2)}(\omega) \vdots \mathbf{P}_{SHG}(\mathbf{r},\omega) \cdot \mathbf{E}_{\mathbf{det}}(\mathbf{r},\omega) dV \tag{3}$$

Where $\mathbf{P}_{SHG}(\mathbf{r}, \omega)$ is the second-order nonlinear optical polarization induced by the incident electric field, and $\mathbf{E}_{\mathbf{det}}(\mathbf{r}, \omega)$ corresponds to a dummy field that is generated by a polarization current at the detector position. More details about the simulations can be found in Experimental Section. The resulting calculated SHG normalized efficiency for the bulk wafer and c-GaP film are shown by the dashed lines in Figure 2a,b, respectively. The model reproduces the shape and features of the measured data with very good agreement, only for the thin film a small deviation can be observed that is probably caused by the high sensitivity of the model to the exact thickness of the sample. The good agreement confirms the previous arguments and indicates a flat dispersion of the second-order nonlinear susceptibility.

However, as mentioned before, the structure of the nonlinear susceptibility $\chi^{(2)}$ is strongly dependent on the symmetries of the nonlinear material. When applying appropriate rotation matrices for [111] oriented GaP, the SHG intensity can expressed in the following form[31](the detailed calculation can be found in Supporting Information):

$$I^{(2)}_{111} \propto (E^2_x E^2_y) + (E^2_x - E^2_y)^2 + (E^2_x + E^2_y)^2 \tag{4}$$

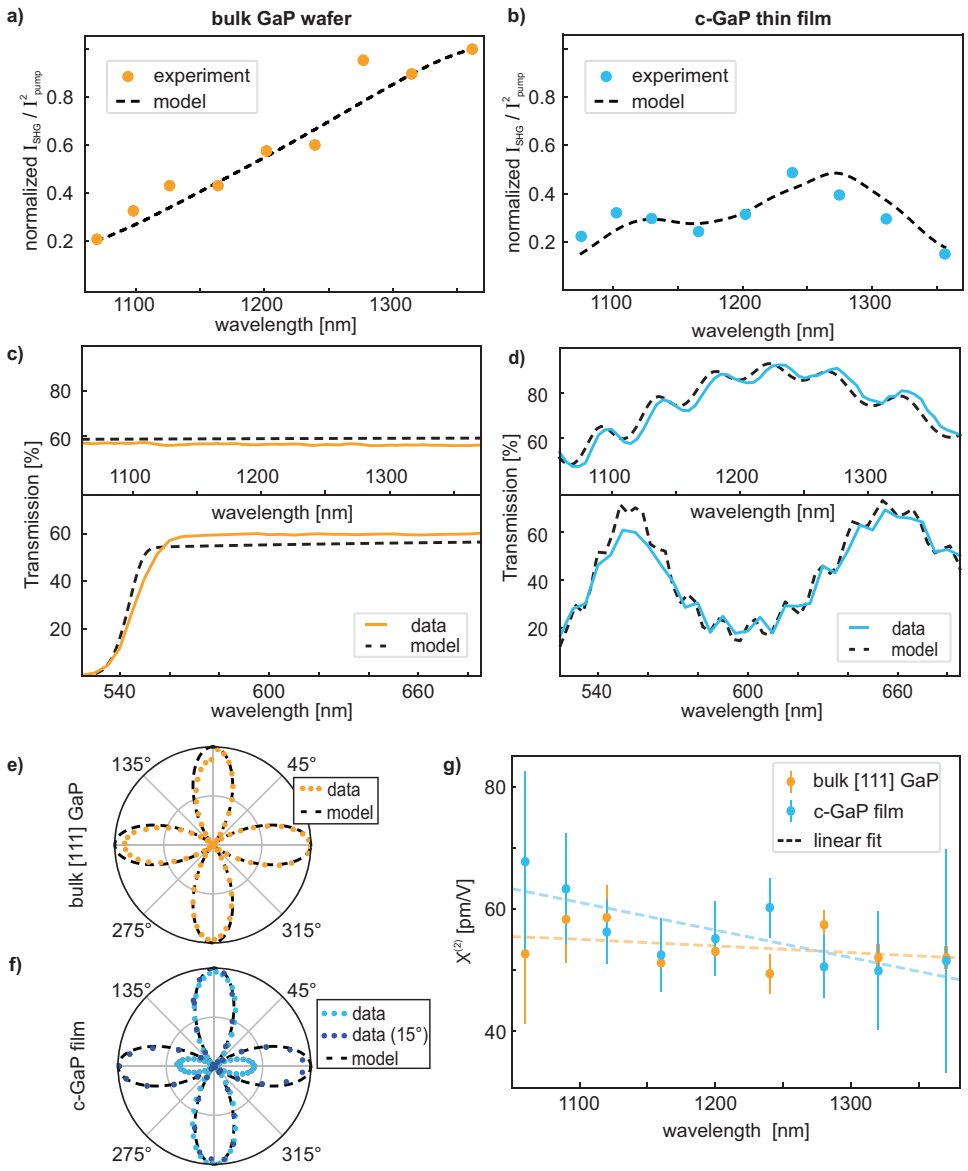

Figure 2. a,b) Power normalized efficiency I_{SHG}/I^2_{pump} of the SHG intensity, extracted from experiments (dots) and simulations (dashed line) for a) the bulk [111] sample and b) the c-GaP film. Both datasets are normalized to the respective maximum value. c,d) Measured (solid line) and simulated (dashed line) transmission spectra for c) bulk and d) c-GaP film. e,f) Polarization measurements from e) bulk and f) GaP thin film. g) Extracted second-order susceptibility values of bulk (orange) and c-GaP thin film (blue). The linear trend is indicated by the dashed lines.

For a normal incident beam (traveling along the *z*-direction), this SHG intensity is constant relative to rotations of the excitation beam polarization. This is experimentally verified by placing a rotable $\lambda/2$ waveplate (*generator*) in the beampath before the sample, as shown in Supporting Information. To further identify the single elements of $P^{(2)}$, a linear polarizer (*analyzer*) is added to the beampath after the SHG light collection. For a fixed horizontal analyzer, the GaP wafer generates a four lobe polarization pattern as shown in Figure 2e. This is in excellent agreement with the horizontal component of the second-order polarization or the first term in Equation 4, shown by the dashed line in Figure 2e. For the c-GaP film, a comparable pattern is shown in Figure 2f (light blue data), however, the lobes in the horizontal direction appear squeezed. This is caused by the oblique growth direction of the c-GaP film, which is confirmed by the fact that a 15° tilting of the sample plane restores the symmetrical shape of the [111] wafer (dark blue data in Figure 2f).

With knowledge of the spectral and polarization dependence of the SHG signal, the value and dispersion of the effective second-order susceptibility $\chi^{(2)}_{\text{eff}}$ can be extracted over the measured spectral range. This is done by comparing the measured normalized SHG intensity with the modeled SHG intensity as defined earlier.

$$\chi^{(2)}_{\text{eff}} \propto \sqrt{\frac{I_{\text{SHG,exp}}/I^2_{\text{pump,exp}}}{I_{\text{SHG,model}}}} \tag{5}$$

Table 1. Second-order nonlinear susceptibility for several nonlinear materials. Shown are the largest values reported. *This work.

Material	Thickness	Wavelength [µm]	$\chi^{(2)}$ [pm V^{-1}]	Reference
GaP	bulk	1.3	53	*
c-GaP	400 nm	1.05–1.4	55	*
MoS_2	bulk	1.56	29	[36]
GaAs	bulk	1.55	120	[39]
BBO	bulk	1.064	3.7	[24]
$LiNbO_3$	bulk	1.5	20-30	[2, 25]
(D)KDP	bulk	1.064	0.39	[24]
$Al_{1-x}Sc_xN$	500 nm	1.54	60	[40]

The results for the GaP crystal (orange) and c-GaP film (blue) are shown in Figure 2g, with the associated error bars resulting from experimental uncertainties, with contribution from the beam waist and power measurements. For both samples, the extracted values range between 50 and 80 pm V^{-1} and roughly follow a linear trend with negative slope. This is expected from Miller's rule,[32] that predicts that the nonlinear susceptibility is related to the dispersion of the linear refractive index, which slowly decreases for longer wavelengths in the case of GaP. The measured value of the nonlinear susceptibility is in reasonable agreement with literature, where it is reported to be 74 pm V^{-1} at 1.313 µm.[24] **Table 1** summarizes the second-order susceptibility of various nonlinear materials. Remarkably, in comparison to most common nonlinear crystals, for example, BBO, (D)KDP, or $LiNbO_3$, the $\chi^{(2)}_{\text{eff}}$ value of GaP exceeds theirs, for the first two by more than one order of magnitude. Although other III–V semiconductors, like for example, GaAs can have larger second-order susceptibility, as high as 370 pm V^{-1},[25] they always suffer from non-negligible absorption over the visible regime. As discussed previously, the linear properties are critical for the SHG efficiency, particularly for thin film materials. Another promising group of nonlinear materials are atomically thin semiconductors, for example, MoS_2,[33] or ReS_2,[34] where huge nonlinear coefficients and nonlinear conversion efficiencies were achieved.[35] However, many of these materials lose their ability for SHG with increasing layer thicknesses[36] and, due to their unique electronic structure commonly suffer from strong linear absorption by excitonic effects[37] which limits their applicability for nanophotonic systems. It should be noted that there are cases, for example, the 3R-phase of MoS_2 where this is not the case and SHG scales with the number of layers.[38]

As mentioned previously, GaP thin films can be alternatively deposited via sputter deposition, which results in an amorphous structure of the material (a-GaP).[18] Since bulk second-order nonlinear processes are not allowed for the centrosymmetric a-GaP film, the nonlinear response is dominated by third-order nonlinear effects. Here, the analogue to SHG is third-harmonic generation (THG), where three incident photons of frequency f_0 get converted into a new photon of triple the original frequency $3\times f_0$. Consequently, THG is described by the third-order nonlinear optical susceptibility:

$$P_i^{(3)} = \chi_{ijkl}^{(3)} E_j E_k E_l \tag{6}$$

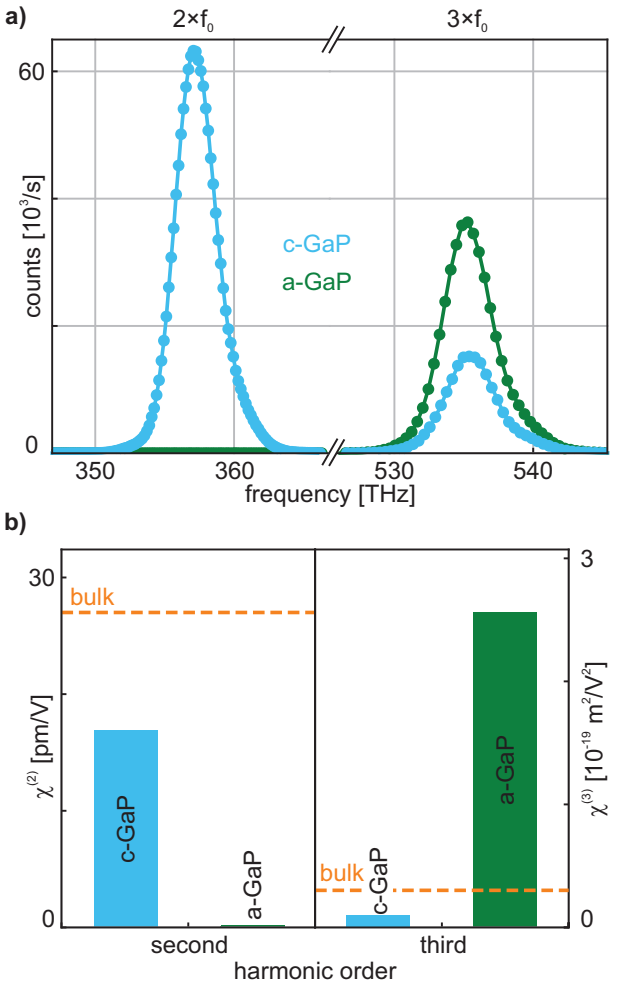

Figure 3. a) Spectra of SHG and THG for the c-GaP (blue) and a-GaP (green) film for a pump frequency of f_0 = 178.4 THz. b) Extracted values of $\chi^{(2)}$ and $\chi^{(3)}$ for the c-GaP (blue) and a-GaP (green) film as well as the bulk GaP crystal (orange dashed line).

Now, $\chi^{(3)}_{ijkl}$ is a rank-4 tensor that contrarily to SHG does not necessarily vanish in centrosymmetric media. In the following, THG measurements are performed with a pump wavelength of λ_0 = 1680 nm (f_0 = 178.4 THz), which was chosen to be larger than triple the value of the electronic bandgap (550 nm) to avoid significant self-absorption of the generated light. **Figure 3**a shows the response of the c-GaP (blue) and a-GaP (green) film under normal incident illumination. Clearly, only the first shows a SHG peak at double the original frequency $2f_0$ = 356.8 THz while both samples exhibit a THG response at $3f_0$ = 535.2 THz. Interestingly, the THG signal of the a-GaP film exceeds the THG signal of the c-GaP film by more than a factor of two, which is opposite to the trend reported for amorphous and crystalline silicon samples.[41] Analogous to the previous procedure, the nonlinear susceptibilities at λ_0 = 1680 nm can be extracted. The resulting values are displayed in Figure 3, for SHG (left panel) and THG (right panel), respectively. For the c-GaP film, $\chi^{(2)}$ calculates to be 16.9pm V^{-1}, which is slightly lower than the ≈ 30 pm V^{-1} achieved for the bulk wafer. Continuing with the third-order

Table 2. Third-order nonlinear optical susceptibility values for selected materials. *This work.

	Thickness	Wavelength [μm]	$\chi^{(3)}$ [10^{-20}m^2/V^2]	Reference
GaP	bulk	1.680	3.015	*
c-GaP	400 nm	1.680	1.0	*
a-GaP	400 nm	1.680	25.6	*
Cuq_2	166 nm	1.064	1.85	[43]
Ge	1.6 μm	1.650	56.5	[44]
Si	bulk	1.650	3.84	[44]
ITO	310 nm	1.24	450	[45]
MoS_2	bulk	1.560	24	[32]

susceptibility, the c-GaP film and wafer reach values in the range of 10^{-20} m^2/V^2 while a-GaP sample outperforms them both by more than one order of magnitude, reaching a value of 25×10^{-20} m^2/V^2. We believe this is mainly caused by two reasons. First, the generalization of Millers rule[42] would predict a higher nonlinear susceptibility based on the slightly higher refractive index of a-GaP compared to the c-GaP. Second, the nonzero absorption coefficient of a-GaP at the pump and the harmonic frequency leads to THG self-absorption that, on the other hand, increases the effective value of $\chi^{(3)}_{\text{eff}}$. In comparison to other nonlinear materials (see **Table 2**), this places a-GaP among the third-order nonlinear materials with the highest nonlinearities, and at the same order of magnitude as, for example, amorphous germanium (Ge) films or 2D materials as molybdenum disulfide (MoS_2). Furthermore, it is only one order of magnitude lower than indium-tin-oxide (ITO) at a very specific condition (epsilon-near zero wavelength at high incidence angle.[25])

Finally, we show that all GaP samples even allow the generation of higher-harmonic (HHG) light. Under illumination with f_0 = 149.9 THz (λ_0 = 2 μm) light, again to reduce self-absorption of the generated signal, up to the fifth-harmonic ($5f_0$ = 749.5 THz) can be observed (see Supporting Information). Thus, the crystalline samples generate light at multiple harmonic-orders (2nd − 5th) while the inversion symmetry of a-GaP prevents the generation of even order harmonics. Therefore, for a-GaP signal can only be observed at the third- and fifth-harmonic of the original frequency.

3. Conclusion

We investigated the nonlinear optical properties of GaP thin films by means of harmonic generation and compared them to the bulk of the same material. We extracted the value of the second-order susceptibility of the crystalline thin film and showed that it is in the same range as bulk GaP crystals. For bulk and c-GaP film, no significant spectral dependence could be measured, in particular no resonance effect when approaching the bandgap of the material. Moreover, the presented results show that the crystalline orientation of the c-GaP film allows efficient SHG under normal incidence illumination and, when correcting for the tilted axis, polarization independent SHG. Finally, we showed that for odd-order nonlinear processes, a-GaP thin films are an alternative that exceeds the efficiencies of the crystalline samples, while providing simpler processing and fabrication flexibility. The extraction of $\chi^{(2)}$ and $\chi^{(3)}$ were carried out with the nonlinear transfer-matrix method. Altogether, we complement the picture of GaP thin films for nonlinear nanophotonic applications with, as we believe, currently one of the most promising combination of high optical coefficients and virtually no losses over most of the visible regime. This paves the way for future applications of GaP thin films, particularly in low-efficiency nonlinear process such as photon-pair generation.

4. Experimental Section

Sample Fabrication: The c-GaP films were fabricated by epitaxial growth on GaAs as wafer. A wafer bonding process and subsequent wet etching of the GaAs results in the desired crystalline GaP film on transparent sapphire substrates. More details on the fabrication can be found published elsewhere.[19,22,23,26] The a-GaP films where fabricated on coverglass substrates (borosilicate) by sputter deposition in an Angstrom deposition tool. During the process, the substrate temperature was kept constant at 350°C. The bulk GaP wafer was purchased from the Institute of Electronic Materials Technology (Warsaw, Poland).

Sample Characterization: XRD measurements were performed using a monochromatic Mo-Kα X-ray beam with λ = 0.71073 Å. The beam was monochromized by a parabolic multilayer, which yields a line focus, that is, a highly parallel beam in horizontal direction with considerable vertical divergence. The surface normal of the samples was aligned in the horizontal plane and rotated around a vertical axis. The diffraction intensities in the horizontal plane were recorded using a Pilatus 100k area detector from Dectris. The measurements were not background corrected. The intensities of the amorphous film (a-GaP) were practically identical to the diffraction signal of its bare substrate, that is, notable Bragg signal was not obsereved from the amorphous GaP film. The other samples show Bragg peaks in accordance with the orientation of the crystalline GaP phase, and in case of the sapphire substrate an additional Bragg peak of the crystalline Al_2O_3 lattice.

Linear optical characterization was performed with an ellipsometer from JA Woolam. Spectral ellipsometry was performed at high incident angles covering the range of 0.3 − 2.0 μm. Additionally, linear transmission measurements at normal incidence were done with the same tool and over the same spectral range. Both datasets were used to extract the linear refractive index for the respective samples.

Nonlinear Optical Measurements: The nonlinear optical measurements were performed with a pulsed laser coupled to an optical parametric amplifier, both by Light Conversion Ltd. The system provides pulses at 100 kHz repetition rate with a temporal pulse with of around 220 fs, covering a wavelength range between 1and1.5 μm. The beam weakly focuses on the sample where the SHG signal was generated (focal length = 300 mm) and the beam size was found using a knife-edge. The generated SHG signal was collected by a visible power meter (Thorlabs, S120VC) with visible shortpass filters to exclude the infra-red pump beam.

For the third-harmonic measurements, a similar laser system was used while the sample was illuminated under stronger focusing (NA = 0.9). An objective (NA = 0.4) was then used to collect the generated signal and send it to a spectrometer with CCD camera (Princeton Instruments). Before, strong filtering makes sure to remove any residual pump signal. The high-harmonic measurements were carried out with an 80 MHz femtosecond Ti:sapphire laser coupled to an optical parametric oscillator (OPO, both by Coherent). By choosing the OPO wavelengths accordingly, an idler wavelength of 2 μm was generated and send to a microscope. There, a high NA objective by Nikon (60x, NA = 0.95) was used to focus on the sample, while another objective (100x, NA = 0.9) was used to collect the light in transmission geometry. Corresponding filters were used to remove the fundamental wavelength, before the generated light was sent to the same spectrometer as for SHG experiments.

Nonlinear Scattering Theory Simulations: The nonlinear simulations were performed by using nonlinear scattering theory in conjunction with

Transfer-Matrix-Method (TMM). Two linear simulations were calculated using (TMM) of the nonlinear polarization at the structure excited by the pump field and the electric field emitted by a dipole source placed at the detector (see Supporting Information).

Supporting Information

Supporting Information is available from the Wiley Online Library or from the author.

Acknowledgements

B.T. and T.H. contributed equally to this work. This work was funded by the Deutsche Forschungsgemeinschaft (DFG, German Research Foundation) under Germany's Excellence Strategy, EXC 2089/1-390776260, and the Bavarian programme Solar Energies Go Hybrid (SolTech). The authors also acknowledge the support of the Center of Nanoscience (CeNS). R.S. and S.V. acknowledge funding from the Engineering and Physical Sciences Research Council (EPSRC) (grant no. EP/V048880). S.A.M. additionally acknowledges the EPSRC (EP/W017075/1), the Leverhulme Trust, the Lee-Lucas Chair in Physics and the Centre of Excellence in Future Low-Energy Electronics Technologies, Australian Research Council (CE170100039).

Open access funding enabled and organized by Projekt DEAL.

Conflict of Interest

The authors declare no conflict of interest.

Data Availability Statement

The data that support the findings of this study are available from the corresponding author upon reasonable request.

Keywords

gallium phosphide, nanophotonics, nonlinear optics, second harmonic generation, thin films

Received: February 2, 2023
Revised: April 20, 2023
Published online: June 2, 2023

[1] Y. R. Shen, in *The Principles of Nonlinear Optics*, Wiley, Hoboken, NJ, USA **1985**.
[2] J. He, H. Chen, J. Hu, J. Zhou, Y. Zhang, A. Kovach, C. Sideris, M. C. Harrison, Y. Zhao, A. M. Armani, *Nanophotonics* **2020**, *9*, 3781.
[3] L. Novotny, B. Hecht, in *Principles of Nano-Optics*, Vol. *9781107005*, Cambridge University Press, Cambridge **2009**.
[4] M. Kauranen, A. V. Zayats, *Nat. Photon.* **2012**, *6*, 737.
[5] N. C. Panoiu, W. E. I. Sha, D. Y. Lei, G.-C. Li, *J. Opt.* **2018**, *20*, 083001.
[6] R. W. Boyd, Z. Shi, I. De Leon, *Opt. Commun.* **2014**, *326*, 74.
[7] Y. Kivshar, *Natl. Sci. Rev.* **2018**, *5*, 144.
[8] K. Koshelev, S. Kruk, E. Melik-Gaykazyan, J.-H. Choi, A. Bogdanov, H.-G. Park, Y. Kivshar, *Science* **2020**, *367*, 288.
[9] F. A. Kish, F. M. Steranka, D. C. DeFevere, D. A. Vanderwater, K. G. Park, C. P. Kuo, T. D. Osentowski, M. J. Peanasky, J. G. Yu, R. M. Fletcher, D. A. Steigerwald, M. G. Craford, V. M. Robbins, *Appl. Phys. Lett.* **1994**, *64*, 2839.
[10] R. Zallen, W. Paul, *Phys. Rev.* **1964**, *134*, 1628.
[11] J. Cambiasso, G. Grinblat, Y. Li, A. Rakovich, E. Cortés, S. A. Maier, *Nano Lett.* **2017**, *17*, 1219.
[12] R. Sanatinia, M. Swillo, S. Anand, *Nano Lett.* **2012**, *12*, 820.
[13] R. Sanatinia, *Ph.D. Thesis*, KTH Royal Institute of Technology, Stockholm, **2014**.
[14] R. Sanatinia, S. Anand, M. Swillo, *Optics Express* **2015**, *23*, 756.
[15] L. Sortino, P. G. Zotev, S. Mignuzzi, J. Cambiasso, D. Schmidt, A. Genco, M. Aßmann, M. Bayer, S. A. Maier, R. Sapienza, A. I. Tartakovskii, *Nat. Commun.* **2019**, *10*, 5119.
[16] L. Sortino, P. G. Zotev, C. L. Phillips, A. J. Brash, J. Cambiasso, E. Marensi, A. M. Fox, S. A. Maier, R. Sapienza, A. I. Tartakovskii, *Nat. Commun.* **2021**, *12*, 6063.
[17] K. Rivoire, A. Faraon, J. Vuckovic, *Appl. Phys. Lett.* **2008**, *93*, 063103.
[18] B. Tilmann, G. Grinblat, R. Berté, M. Özcan, V. F. Kunzelmann, B. Nickel, I. D. Sharp, E. Cortés, S. A. Maier, Y. Li, *Nanoscale Horiz.* **2020**, *5*, 1500.
[19] G. Grinblat, H. Zhang, M. P. Nielsen, L. Krivitsky, R. Berté, Y. Li, B. Tilmann, E. Cortés, R. F. Oulton, A. I. Kuznetsov, S. A. Maier, *Sci. Adv.* **2020**, *6*, eabb3123.
[20] D. J. Wilson, K. Schneider, S. Hönl, M. Anderson, Y. Baumgartner, L. Czornomaz, T. J. Kippenberg, P. Seidler, *Nat. Photon.* **2020**, *14*, 57.
[21] G. Q. Moretti, E. Cortés, S. A. Maier, A. V. Bragas, G. Grinblat, *Nanophotonics* **2021**, *10*, 4261.
[22] A. P. Anthur, H. Zhang, R. Paniagua-Dominguez, D. A. Kalashnikov, S. T. Ha, T. W. W. Maß, A. I. Kuznetsov, L. Krivitsky, *Nano Lett.* **2020**, *20*, 8745.
[23] M. R. Shcherbakov, H. Zhang, M. Tripepi, G. Sartorello, N. Talisa, A. AlShafey, Z. Fan, J. Twardowski, L. A. Krivitsky, A. I. Kuznetsov, E. Chowdhury, G. Shvets, *Nat. Commun.* **2021**, *12*, 10.
[24] I. Shoji, T. Kondo, R. Ito, *Opt. Quantum Electron.* **2002**, *1961*, 797.
[25] R. W. Boyd, in *Nonlinear Optics*, 3rd ed., Elsevier, Amsterdam, ISBN 9780123694706, **2008**, pp. 1–67.
[26] A. P. Anthur, H. Zhang, Y. Akimov, J. Rong Ong, D. Kalashnikov, A. I. Kuznetsov, L. Krivitsky, *Opt. Express* **2021**, *29*, 10307.
[27] K. Persson, Materials Data on GaP (SG:216) by Materials Project Materials Data Project. *Materials Data on GaP by Materials Project*. United States: N. p., **2020**, https://doi.org/10.17188/1200314.
[28] J. D. Sautter, L. Xu, A. E. Miroshnichenko, M. Lysevych, I. Volkovskaya, D. A. Smirnova, R. Camacho-Morales, K. Zangeneh Kamali, F. Karouta, K. Vora, H. H. Tan, M. Kauranen, I. Staude, C. Jagadish, D. N. Neshev, M. Rahmani, *Nano Letters* **2019**, *19*, 3905.
[29] Z. H. Amber, B. Kirbus, L. M. Eng, M. Rüsing, *J. Appl. Phys.* **2021**, *130*, 133102.
[30] K. O'Brien, H. Suchowski, J. Rho, A. Salandrino, B. Kante, X. Yin, X. Zhang, *Nat. Mater.* **2015**, *14*, 379.
[31] R. Yi, X. Zhang, C. Li, B. Zhao, J. Wang, Z. Li, X. Gan, L. Li, Z. Li, F. Zhang, L. Fang, N. Wang, P. Chen, W. Lu, L. Fu, J. Zhao, H. H. Tan, C. Jagadish, *Light Sci. Appl.* **2022**, *11*, 1.
[32] R. C. Miller, *Appl. Phys. Lett* **1964**, *5*, 17.
[33] J. Zhang, W. Zhao, P. Yu, G. Yang, Z. Liu, *2D Mater.* **2020**, *7*, 042002.
[34] Y. Song, S. Hu, M.-L. Lin, X. Gan, P.-H. Tan, J. Zhao, *ACS Photon.* **2018**, *5*, 3485.
[35] I. Abdelwahab, B. Tilmann, Y. Wu, D. Giovanni, I. Verzhbitskiy, M. Zhu, R. Berté, F. Xuan, L. D. S. Menezes, G. Eda, T. C. Sum, S. Y. Quek, S. A. Maier, K. P. Loh, *Nat. Photon.* **2022**, *16*, 644.
[36] R. I. Woodward, R. T. Murray, C. F. Phelan, R. E. P. de Oliveira, T. H. Runcorn, E. J. R. Kelleher, S. Li, E. C. de Oliveira, G. J. M. Fechine, G. Eda, C. J. S. de Matos, *2D Mater.* **2016**, *4*, 011006.
[37] G. A. Ermolaev, Y. V. Stebunov, A. A. Vyshnevyy, D. E. Tatarkin, D. I. Yakubovsky, S. M. Novikov, D. G. Baranov, T. Shegai, A. Y. Nikitin, A. V. Arsenin, V. S. Volkov, *npj 2D Mater. Appl.* **2020**, *4*, 21.
[38] M. Zhao, Z. Ye, R. Suzuki, Y. Ye, H. Y. Zhu, J. Xiao, Y. Wang, Y. Iwasa, X. Zhang, *Light Sci. Appl.* **2016**, *5*, e16131.

[39] I. Shoji, A. Kitamoto, T. Kondo, R. Ito, in *Pro. of 5th Eur. Quant. Electr. Conf.*, Vol. *14*. IEEE, ISBN 0-7803-1791-2, **1994** pp. 263–263.
[40] V. Yoshioka, J. Lu, Z. Tang, J. Jin, R. H. Olsson, B. Zhen, *APL Mater.* **2021**, *9*, 101104.
[41] C. C. Wang, J. Bomback, W. T. Donlon, C. R. Huo, J. V. James, *Phys. Rev. Lett.* **1986**, *57*, 1647.
[42] W. Ettoumi, Y. Petit, J. Kasparian, J.-P. Wolf, *Opt. Express* **2010**, *18*, 6613.
[43] A. Popczyk, A. Aamoum, A. Migalska-Zalas, P. Płóciennik, A. Zawadzka, J. Mysliwiec, B. Sahraoui, *Nanomaterials* **2019**, *9*, 254.
[44] G. Grinblat, Y. Li, M. P. Nielsen, R. F. Oulton, S. A. Maier, *Nano Lett.* **2016**, *16*, 4635.
[45] M. Z. Alam, I. De Leon, R. W. Boyd, *Science* **2016**, *352*, 795.